Magn Reson Med Sci 2018; 17; 21–27
doi:10.2463/mrms.mp.2016-0136
Published Online: May 18, 2017

MAJOR PAPER

Utility of a Hybrid IVIM-DKI Model to Predict the Development of Distant Metastasis in Head and Neck Squamous Cell Carcinoma Patients

Noriyuki Fujima[1*], Tomohiro Sakashita[2], Akihiro Homma[2], Daisuke Yoshida[1], Kohsuke Kudo[1], and Hiroki Shirato[3,4]

Purpose: To evaluate the diagnostic power of hybrid intravoxel incoherent motion (IVIM)-diffusion kurtosis imaging (DKI) model parameters in pretreatment for the prediction of future distant metastasis in head and neck squamous cell carcinoma (HNSCC) patients.

Materials and Methods: We retrospectively evaluated 49 HNSCC patients who underwent curative chemoradiation therapy. Diffusion-weighted image (DWI) acquired by single-shot spin-echo echo-planar imaging with 12 b-values (0–2000) was performed in all patients before any treatment. We calculated the IVIM-DKI parameters and the conventional apparent diffusion coefficient (ADC) in the ROI placed on the primary lesion. The presence of future distant metastasis was determined by histological findings or clinical follow-up.

Results: A univariate analysis revealed significant differences between the patients with distant metastasis and those without in slow diffusion coefficient (D) and kurtosis value (K). Highest diagnostic accuracy was obtained by the D value. In addition, a multivariate analysis revealed that the D value was an independent predictor of future distant metastasis.

Conclusion: The D and K values obtained by this hybrid IVIM-DKI model can be one of the diagnostic tools for the prediction of future distant metastasis in HNSCC patients.

Keywords: *diffusion-weighted imaging, intravoxel incoherent motion, diffusional kurtosis imaging, head and neck squamous cell carcinoma*

Introduction

Distant metastasis is one of the major causes of poor outcomes in patients with a malignant lesion, including head and neck squamous cell carcinoma (HNSCC). Advances in treatment methods such as a combination of surgery, chemotherapy and radiotherapy have led to improved local control of primary lesions such as sinonasal cavity or pharynx squamous cell carcinomas (SCCs).[1–3] However, patients may develop distant metastasis after treatment, even if the primary lesion was successfully controlled.[4] In addition, systematic screening by whole-body scanning using CT or ^{18}F-fluorodeoxyglucose (FDG) positron-emission tomography (PET)/CT at short intervals can be used to detect distant metastases in HNSCC patients after the curative treatment, but this may not be cost-effective. Therefore, predictors of the occurrence of future distant metastasis are needed before the follow-up period.

In previous studies, several factors were related to the incidence rate of distant metastasis, such as T-stage, N-stage, the presence of extra-nodal spread, histological differentiation, the achievement of local control by the initial curative treatment, history of continued smoking after treatment, and the patients' specific genomic information before the treatment.[5–11] However, the diagnostic power varies among these reports. In addition, several factors related to histological information required the performance of an invasive surgical

[1]Department of Diagnostic and Interventional Radiology, Hokkaido University Hospital, N15, W7, Kita-Ku Sapporo, Hokkaido 060-8638, Japan
[2]Department of Otolaryngology-Head and Neck Surgery, Hokkaido University Graduate School of Medicine, Hokkaido, Japan
[3]Department of Radiation Medicine, Hokkaido University Graduate School of Medicine, Hokkaido, Japan
[4]The Global Station for Quantum Medical Science and Engineering, Global Institution for collaborative research and education, Hokkaido, Japan

*Corresponding author, Phone: +81-11-706-5977, Fax: +81-11-706-7876, E-mail: Noriyuki.Fujima@mb9.seikyou.ne.jp

Received: November 25, 2016 | Accepted: March 29, 2017

procedure, and the information of genomic status was not always available. Additional supporting information will be also required to elevate the diagnostic power.

Diffusion-weighted imaging (DWI) obtained by MRI is an imaging technique that reflects tissue microstructural information by depicting the microscopic-level water diffusivity in the tissue. By using monoexponential fitting to the obtained signal in DWI, water diffusivity has been semi-quantitatively assessed as the value of apparent diffusion coefficient (ADC). In recent years, advanced fitting models for diffusion-weighted MRI such as intravoxel incoherent motion (IVIM) and diffusional kurtosis imaging (DKI) were reported for the non-invasive visualization of tissue structural information.[12–16] A method for the simultaneous calculation of IVIM and DKI parameters was recently described as a hybrid IVIM and DKI model.[17] The information obtained by IVIM can simultaneously detect both fast diffusion (which may reflect the perfusion related diffusion) and slow diffusion (which may reflect the tissue related diffusion).[18] DKI was described to detect the information related to the microstructural tissue heterogeneity.[19] Such information can well describe the tumor characteristics and provide important clues to a patient's prognosis. The utility of these techniques for the prediction of treatment outcomes in patients with HNSCC has been recently described in a few reports.[20–22] Such microstructural information can also be used to help predict the development of distant metastasis in HNSCC patients. Our goal in the present study was to determine the diagnostic power of hybrid IVIM-DKI model parameters in pretreatment for the prediction of distant metastasis in HNSCC patients.

Patients and Methods

Study population

The protocol of this retrospective study was approved by our institutional review board, and written informed consent was waived. We evaluated the 49 patients with HNSCC who were treated at our hospital from October 2010 to October 2015. All patients fulfilled the following inclusion criteria: 1) histopathological diagnosis of SCC, 2) the patient had received a full course of curative chemoradiation therapy, 3) MRI including multiple b-value DWI was performed before any treatment, and 4) no distant metastasis was present at the pretreatment stage, confirmed by whole-body CT and PET/CT. The characteristics of the 49 patients were as presented in Table 1. The histopathological diagnosis was SCC in all patients. The treatment regimen was a super-selective arterial infusion of cisplatin with concomitant radiotherapy for all patients. The patients' treatment details were as follows: an arterial infusion of cisplatin (100–120 mg/m^2 per week for 4 weeks) to the primary tumor's dominant blood supply, using a microcatheter, with concurrent radiotherapy of a total of 70 Gy in 35 fractions.

The determination of distant metastasis

In all patients, clinical and radiological follow-ups were performed after the treatment to determine the final diagnosis related to the presence of distant metastasis. In all patients, follow-up CT with the scan interval of 3–12 months and PET/CT with the scan interval of 6–12 months were respectively performed for the detection of distant metastasis. The CT scanning included the scan range of the chest and upper abdomen, and the PET/CT included the whole body. The strategy for identifying the presence/absence of distant metastasis was as follows. (1. Histological determination of the suspected lesion; (2. Appearance of multiple new lesions in the organ (especially lung) detected by CT or PET/CT and the constant development of these lesions. The follow-up period in each patient was ≥1 year (the minimum follow-up period was set as 1 year). If any newly developed mass lesion was not detected by the follow-up CT or PET/CT during the entire follow-up period, the patient was classified as being in the non-distant metastasis group.

Table 1. Patient characteristics (n = 49)

	Number of patients
Age	
Range	46–77
Median	61
Average	60.6
Gender	
Male	42
Female	7
Primary tumor site	
Nasal cavity	4
Sinonasal cavity	25
Oropharynx	17
Hypopharynx	3
T-stage	
T1	0
T2	6
T3	14
T4a	22
T4b	7
N-stage	
N0	31
N1	5
N2a	1
N2b	7
N2c	5
N3	0

Magnetic Resonance Imaging Protocol

DWI

All MR imaging was performed using a 3.0 Tesla unit (Achieva TX; Philips Healthcare, Best, Netherlands) with a 16-channel neurovascular coil. The DWI acquisition used single-shot spin-echo echo-planar imaging (EPI) with three orthogonal motion probing gradients. Twelve b-values (0, 10, 20, 30, 50, 80, 100, 200, 400, 800, 1000, and 2000 s/mm^2) were used. Diffusion images were acquired with a three-directional trace scheme for each b-value. The other imaging parameters were: TR, 4500 ms; TE, 64 ms; DELTA (large delta; gradient time interval), 30.1 ms; delta (small delta; gradient duration), 24.3 ms; flip angle, 90°; FOV, 230 × 230 mm; 64 × 64 matrix; slice thickness, 5 mm × 20 slices; voxel size 3.59 × 3.59 × 5.00 mm; parallel imaging acceleration factor, 2; the number of signal averages = b-value of 0–100 s/mm^2 (one average), 200–800 s/mm^2 (two averages) and 1000–2000 s/mm^2 (three averages); scanning time, 4 min 37 s. In this sequence, for the reduction of image distortion in EPI, low in-plane matrix combined with the parallel imaging technique were applied to decrease the number of EPI factor as possible, as described above. Patients were instructed not to swallow, move their tongues, open their mouths, or make any other voluntary motion before DWI scanning. In addition, their heads were fixed firmly with the coil to prevent movement during scanning.

Conventional MRI

Conventional MRI was also obtained to evaluate the primary tumor. These images included (a) an axial T_1-weighted image (T_1WI) with a spin-echo sequence (TR, 450 ms; TE, 10 ms; FOV, 240 × 240 mm; 512 × 512 matrix; slice thickness, 5 mm; inter-slice gap, 30%; scanning time, 2 min 12 s) and (b) an axial T_2-weighted image (T_2WI) with a turbo spin-echo (TSE) sequence with fat suppression (TR, 4500 ms; TE, 70 ms; TSE factor, 9; FOV, 240 × 240 mm; 512 × 512 matrix; slice thickness, 5 mm; inter-slice gap, 30%; scanning time, 2 min 06 s).

Data analysis

From the diffusion signal data, we calculated each parameter of hybrid bi-exponential function (the perfusion fraction [*f*], the pseudo-diffusion coefficient [*D**], the true diffusion coefficient [*D*], and the kurtosis value [*K*]) by using the signal intensity of all 12 b-values. To perform these parameter calculations, we used the following equation:[17]

$$\frac{S_{(b)}}{S_0} = f \times \exp(-b \times D^*) + (1-f) \times \exp\left(-b \times D + \frac{1}{6} \times b^2 \times D^2 \times K\right) \quad [1]$$

where $S_{(b)}$ is the signal intensity at the b-value denoted by the subscript, S_0 is the signal intensity at the b-value of 0, and *b* is b-factor in Eq. [1]. We fitted the signal intensity of b-values in Eq. [1] with least-square fitting using the Levenberg-Marquardt algorithm. All parameter calculations were performed using the mean signal intensity based on the ROIs. To improve the fitting accuracy and to prevent overfitting in all b-value fitting analyses of the hybrid bi-exponential models, we performed the fitting procedure by the following methods. In the bi-exponential analysis, first, the data of b > 200 s/mm^2 were fitted for the calculation of parameters *D* and *K*. In the second step, the curve was fitted for *f* and *D** over all b-values by using Eq. [1], while keeping *D* and *K* constant. We also calculated the conventional ADC using two b-values (0 and 1000). The following equation was used for the ADC calculation:

(Signal intensity of b = 1000) /
(Signal intensity of b = 0) = exp(−1000*ADC)

ROI delineation and parameter calculations

Each tumor was delineated with a polygonal ROI on b_0 images of the DWI in the analysis by a board-certified neuroradiologist with 19 years of experience. T_1WI and T_2WI were used as reference images for the delineation. Each b-value imaging datum, especially high b-value images, was also used to help detect the tumor's solid component with reference to the ROI delineation. In addition, strong high-signal areas on the EPI-b_0 image and T_2WI which suggested necrosis or cyst formation were excluded from the ROI. The tumor ROI was then copied in the EPI images of the DWI for each b-value (Fig. 1). If the tumor extended into two or more slices, the slice with the largest depiction of the tumor was used for the parameter calculation. The DWI model parameter calculation was performed by the ROI-based approach for the analysis because the calculation process can be performed with a high signal-to-noise ratio (SNR)[12]. In the ROI-based approach, the IVIM parameter and the ADC calculations were performed as follows: 1) the mean value of each ROI in the multi b-value EPI was defined as the image signal intensity for each b-value, and 2) by using the mean signal intensity in the ROI for each b-value, the IVIM parameters were calculated using the two-step fitting as described above, and the ADC value was also calculated by simple linear fitting. In addition, to assess the goodness of fit in the IVIM/DKI model fitting, we calculated the coefficient of determination (R^2 value; $R^2 = 1 - ESS/TSS$, where ESS is the sum of the squared errors between the data points and the IVIM/DKI model fitting curve, and TSS is the sum of the squared differences between the data points and the mean value of all data points) in each tumor.

Statistical analysis

In a univariate analysis, we used the univariate logistic regression analyses to compare the pretreatment T-stage (T1–2 vs. T3–4), N-stage (N0–1 vs. N2–3), primary site (nasal or sinonasal vs. pharynx), presence/absence of local control, and the five diffusion parameters (ADC, *f*, *D**, *D* and *K*) between the patients with future distant metastasis

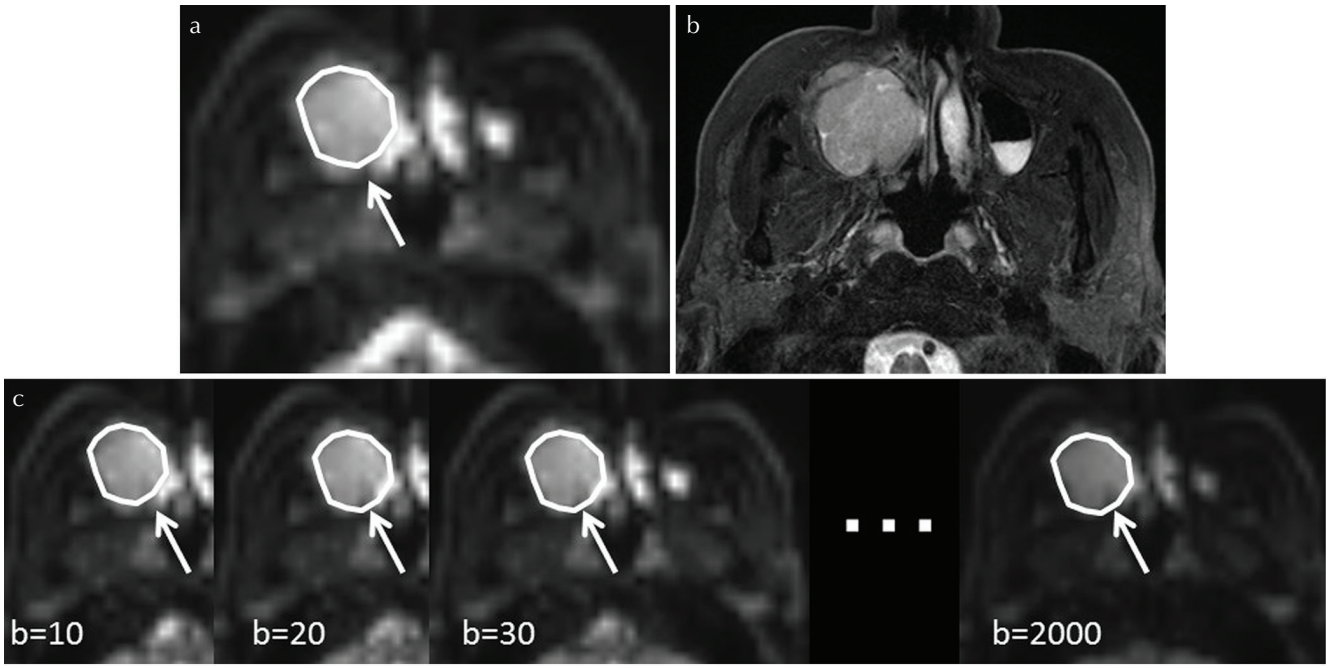

Fig. 1 Tumor ROI delineation. Each primary tumor was outlined by a polygonal ROI on b_0 images of diffusion weighted image (DWI) (**a**, arrow). T_2-weighted images (T_2WI) (**b**) were used as reference images for the ROI delineation. The tumor ROI was then copied on the echo-planar imaging (EPI) of the respective b-values (**c**, arrows).

and those without it. If a statistical significance was obtained for more than two parameters among all parameters, these parameters were further analyzed by multivariate logistic regression models to determine whether they had independent predictive value with odds ratios and corresponding 95% confidence intervals. The detected predictive values were also assessed using receiver operating characteristic (ROC) curves constructed for calculating the area under the curve (AUC). We determined the sensitivity, specificity, positive predictive value, negative predictive value and diagnostic accuracy by using the highest Youden index (Sensitivity + Specificity − 1). *P*-values < 0.05 were considered significant. SPSS software (IBM, Armonk, NY, USA) was used for all analyses.

Results

Among the 49 patients, ten metastatic lesions in eight patients were discovered during the follow-up period. The site of the metastasis was lung in seven patients, bone in one patient, kidney in one patient and liver in one patient. The distant metastasis of a kidney lesion in one patient was confirmed by histological resection, and the other distant metastases were all confirmed by clinical follow-up by CT and PET/CT (mean 26 mos; range 12–52 mos).

We successfully obtained DWI parameters for the pretreatment primary tumor in all 49 patients. The patients' characteristics, the details of the IVIM-DKI parameters and the ADC of the patients with distant metastasis and those without are presented in Table 2. The univariate logistic regression analyses revealed statistical significance in both the *D* and *K* values between the patients with distant metastasis and those without. From the ROC curve analysis, we calculated the AUC, sensitivity, specificity, positive predictive value, negative predictive value, accuracy and cut-off value (Table 3). Notably, the negative predictive value of *D* was the highest (=0.94).

The multivariate logistic regression analyses revealed that the D value was an independent predictor of distant metastasis ($P = 0.009$). The odds ratio was determined 2.28 with the range of 95% confidence intervals of 0.01–9.78. In contrast, the *K* value was revealed it was not significant parameter as a predictor of the distant metastasis ($P = 0.39$). The odds ratio of *K* was 0.06 with the range of 95% confidence intervals of 0.0001–24.5. The results of the univariate and multivariate logistic regression analyses are summarized in Table 4.

In the fitting of each tumor ROI, the coefficient of determination (R^2 value) was 0.96 ± 0.03. Figure 2 presents a case example of a directly obtained DWI signal intensity plot and the fitting curve.

Discussion

Our present findings demonstrated a significant difference in the slow diffusion coefficient *D* and the kurtosis value *K* obtained by the hybrid IVIM-DKI diffusion model between patients who are predicted to develop distant metastasis and those who are not predicted to develop metastasis. Several studies have described indicators that have a relationship to future distant metastasis,[5–11] but the indicators differed among

Table 2. Patient characteristics and parameters of the patients with and without predicted distant metastasis

			Presence of future distant metastasis	
			metastasis (+)	metastasis (–)
Patients' characteristics (no. of patients)	T-stage	T1 or 2	0	6
		T3 or 4	8	35
	N-stage	N0 or 1	4	32
		N2 or 3	4	9
	Location	nasal/sinonasal	3	26
		pharynx	5	15
	Local control/ failure	local control	4	32
		local failure	4	8
IVIM-DKI parameter (parameter value)	*f* (% ×10^2)		0.11 ± 0.02	0.12 ± 0.05
	*D** (mm^2/s)		17.7 ± 5.6	20.7 ± 8.9
	D (mm^2/s)		0.82 ± 0.08	0.96 ± 0.12
	K		0.91 ± 0.08	0.82 ± 0.1
ADC (parameter value)	ADC (mm^2/s)		0.97 ± 0.09	1.07 ± 0.13

The data of intravoxel incoherent motion (IVIM)-diffusion kurtosis imaging (DKI) parameters and the ADC are mean ± standard deviation (SD). D, true diffusion coefficient (×10^{-3} mm^2/s); *f*, perfusion fraction (×10^2%); *D**, fast diffusion coefficient (×10^{-3} mm^2/s); *K*, kurtosis value (dimensionless); ADC, apparent diffusion coefficient (×10^{-3} mm^2/s).

Table 3. ROC analysis results

Parameter	AUC	Sensitivity	Specificity	PPV	NPV	Accuracy	Cut-off value
D	0.808	0.78	0.76	0.41	0.94	0.76	0.85
K	0.767	0.75	0.68	0.31	0.93	0.69	0.88

AUC, area under curve; PPV, positive predictive value; NPV, negative predictive value; D, true diffusion coefficient (×10^{-3} mm^2/s); K, kurtosis value (dimensionless).

Table 4. Univariate and multivariate analysis results

	Univariate analysis	
	Odds ratio	*P*-value
T-stage	0.19 (0.009, 19.41)	0.071
N-stage	2.28 (0.01, 9.78)	0.11
Location of primary site	3.56 (0.73, 17.11)	0.18
Local control/failue	3.55 (0.73, 17.1)	0.11
f	0.21 (0.08, 0.69)	0.51
*D**	0.94 (0.84, 1.05)	0.35
D	6.13 (3.24, 24.52)	0.0015*
K	4.31 (3.2, 19.45)	0.028*
ADC	3.82 (1.51, 17.85)	0.061
	Multivariate analysis	
	Odds ratio	*P*-value
D	2.28 (0.01, 9.78)	0.009*
K	0.06 (0.0001, 24.5)	0.39

The odds ratio data in parentheses are 95% confidence intervals. *P* value with * mean statistical significance. D, true diffusion coefficient (×10^{-3} mm^2/s); f, perfusion fraction (×10^2%); D*, fast diffusion coefficient (×10^{-3} mm^2/s); K, kurtosis value (dimensionless); ADC, apparent diffusion coefficient (×10^{-3} mm^2/s).

these reports, and several factors that were revealed by one study were not confirmed as a predictor in another study. The patient characteristics and treatment details of the prior studies may have affected the results, and the true predictors have remained unclear. Notably, no quantitative noninvasive imaging parameter has been reported as a predictor of future distant metastasis in HNSCC patients. The present study's results indicate that parameters obtained by the advanced diffusion model of IVIM-DKI can be used as a diagnostic tool for the detection of high-risk patients who may suffer from future distant metastasis. The prediction of a tendency to develop distant metastases will also be useful information for the determination of the interval of clinical routine examinations. Adjustments of follow-up strategies by using diffusion parameters can influence the patients' quality of life and reduce healthcare costs.

In the current study, multivariate analysis revealed that the *D* value was an independent predictor for the future development of distant metastasis. In regard to the tumor microstructural information such as histological features, in general, histological poorly differentiated SCCs tend to grow rapidly, and the prevalence rate of distant metastasis among these SCCs was rather higher than that of well-differentiated cases.[8,11] Information obtained by DWI is generally said to

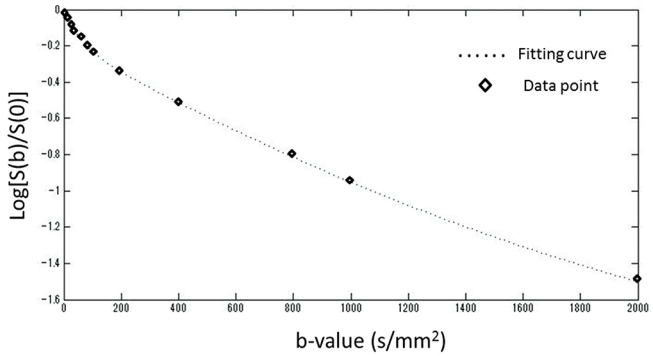

Fig. 2 Hybrid intravoxel incoherent motion (IVIM)-diffusion kurtosis imaging (DKI) model fitting curves with diffusion-weighted image (DWI)-signal plots. Representative fitting curves of the IVIM-DKI hybrid model to all b-value signal data was presented.

reflect the tissue microstructural information indirectly by depicting the degree of water diffusivity in the tumor tissue. Yun et al. reported that the ADC is correlated with the histological differentiation in HNSCCs.[23] In another report, the ADC had a significant correlation with the tumor cell density.[24] These reports indicate that the ADC can reflect a certain degree of microstructural characteristics in tumor tissue. In addition, the *D* value obtained by the IVIM model was considered more sensitive to the tissue diffusion because the IVIM model divided the fast and slow diffusion components, since pure slow diffusion can be measured by excluding the fast diffusion (perfusion-related diffusion) signal. Therefore, the *D* value might reflect the tissue characteristics more than the ADC. The *D* value may be related to the tumor microstructural information such as the tumor's histological differentiation, and thus this parameter might be related to the occurrence rate of future distant metastasis. However, we did not determine the correlation between histological differentiation and diffusion parameters in the current study. The histological diagnoses were obtained by biopsy tissue for all patients, and the diagnosis of several patients was made using a very small tumor fragment; we suspect that such small tumor tissue did not necessarily reflect the entire tumor's differentiation because of intratumoral heterogeneity. To clarify this issue, future studies are needed to compare diffusion parameters and the tumor histological differentiation diagnosed from a sufficient volume of tumor tissue (e.g., by surgical total or subtotal resection).

Our present study's univariate analysis also revealed that the *K* value was significantly higher in the patients who were predicted to develop distant metastasis, although it was not significant in the multivariate analysis. It is still unclear what tumor tissue characteristic is reflected by this value. Other research groups have speculated that this value might reflect aspects of tissue complexity such as cell shape and size, the balance of extracellular extravascular space and cellular space, and other tissue structural information.[19,21] Although the relationships among such information and the prevalence of future distant metastasis remains unclear, the *K* value may reflect the microstructural complexity and its information that are indirectly related to the tumor aggressiveness or the tendency of tumor spread from the primary site and the rate of the occurrence of future distant metastasis.

Our study has several limitations. First, it was a retrospective study, and thus a fixed b-value was used only for the diffusion signal analysis. The appropriate arrangement of b-values for the short scanning time with the sufficient reliability was unclear. In addition, diffusion model parameters can vary if a different arrangement of b-values is used. We used a fixed b-value, however, diffusion parameters examined using other b-value arrangements may have higher predictive power for future distant metastasis. To address these limitations, further analyses are needed. Second, we did not assess the reproducibility when we performed the calculations with the advance diffusion model. The scan-rescan variability can change the diagnostic power of diffusion parameters, and thus further analyses are needed for this issue too. Third, the number of patients was small. There were only eight patients with future distant metastasis, because the frequency of distant metastasis in HNSCC patients is not necessarily high. A detailed subgroup analysis with large number of patients is needed for the determination of *D* and *K* values as predictors for the future distant metastasis, dividing the patients into groups based on the primary lesion, the metastasis site, the TNM stage and the presence of local control. In addition, the diagnostic power of diffusion parameters as a general prognostic factor should be determined by comparing the overall survival rate, and also the degree of relation to the respective sub-categorized prognosis-related factors such as the presence of local control, future distant metastasis, and other factors that may affect the overall survival rate, in analyses of larger numbers of patients. In such analyses, the follow-up period should be longer (e.g., ≥2 years after the treatment), especially when the prediction of future distant metastasis is being assessed.

Conclusion

The D and the K values obtained using IVIM-DKI model can be one of the diagnostic tools used for the prediction of future distant metastasis in HNSCC patients. By using this technique, the follow-up strategy can be modified based on the individual patient's diffusion parameter values obtained using the hybrid IVIM-DKI model.

Acknowledgment

The first author (Noriyuki Fujima) has received the grant support from Ministry of Education, Culture, Sports, Science and Technology–Japan (ID; 15K19761).

Conflicts of Interest

We declare that we have no conflict of interest.

References

1. Pignon JP, Bourhis J, Domenge C, Designé L. Chemotherapy added to locoregional treatment for head and neck squamous-cell carcinoma: three meta-analyses of updated individual data. Lancet 2000; 355:949–955.
2. Homma A, Sakashita T, Yoshida D, et al. Superselective intra-arterial cisplatin infusion and concomitant radiotherapy for maxillary sinus cancer. Br J Cancer 2013; 109:2980–2986.
3. Sakashita T, Homma A, Hatakeyama H, et al. Salvage operations for patients with persistent or recurrent cancer of the maxillary sinus after superselective intra-arterial infusion of cisplatin with concurrent radiotherapy. Br J Oral Maxillofac Surg 2014; 52:323–328.
4. Pulte D, Brenner H. Changes in survival in head and neck cancers in the late 20th and early 21st century: a period analysis. Oncologist 2010; 15:994–1001.
5. Madana J, Morand GB, Alrasheed A, et al. Clinical parameters predicting development of pulmonary malignancies in patients treated for head and neck squamous cell carcinoma. Head Neck 2016; 38 Suppl 1:E1277–E1280.
6. Lallemant B, Evrard A, Chambon G, et al. Gene expression profiling in head and neck squamous cell carcinoma: Clinical perspectives. Head Neck 2010; 32:1712–1719.
7. Rickman DS, Millon R, De Reynies A, et al. Prediction of future metastasis and molecular characterization of head and neck squamous-cell carcinoma based on transcriptome and genome analysis by microarrays. Oncogene 2008; 27:6607–6622.
8. Coca-Pelaz A, Rodrigo JP, Suárez C. Clinicopathologic analysis and predictive factors for distant metastases in patients with head and neck squamous cell carcinomas. Head Neck 2012; 34:771–775.
9. León X, Quer M, Orús C, del Prado Venegas M, López M. Distant metastases in head and neck cancer patients who achieved loco-regional control. Head Neck 2000; 22:680–686.
10. Al-Othman MO, Morris CG, Hinerman RW, Amdur RJ, Mendenhall WM. Distant metastases after definitive radiotherapy for squamous cell carcinoma of the head and neck. Head Neck 2003; 25:629–633.
11. Liao CT, Wang HM, Chang JT, et al. Analysis of risk factors for distant metastases in squamous cell carcinoma of the oral cavity. Cancer 2007; 110:1501–1508.
12. Fujima N, Yoshida D, Sakashita T, et al. Intravoxel incoherent motion diffusion-weighted imaging in head and neck squamous cell carcinoma: assessment of perfusion-related parameters compared to dynamic contrast-enhanced MRI. Magn Reson Imaging 2014; 32:1206–1213.
13. Marzi S, Piludu F, Vidiri A. Assessment of diffusion parameters by intravoxel incoherent motion MRI in head and neck squamous cell carcinoma. NMR Biomed 2013; 26:1806–1814.
14. Marzi S, Stefanetti L, Sperati F, Anelli V. Relationship between diffusion parameters derived from intravoxel incoherent motion MRI and perfusion measured by dynamic contrast-enhanced MRI of soft tissue tumors. NMR Biomed 2016; 29:6–14.
15. Xu XQ, Choi YJ, Sung YS, et al. Intravoxel incoherent motion MR imaging in the head and neck: correlation with dynamic contrast-enhanced MR imaging and diffusion-weighted imaging. Korean J Radiol 2016; 17:641–649.
16. Fujima N, Sakashita T, Homma A, et al. Advanced diffusion models in head and neck squamous cell carcinoma patients: goodness of fit, relationships among diffusion parameters and comparison with dynamic contrast-enhanced perfusion. Magn Reson Imaging 2017; 36:16–23.
17. Wu WC, Yang SC, Chen YF, Tseng HM, My PC. Simultaneous assessment of cerebral blood volume and diffusion heterogeneity using hybrid IVIM and DK MR imaging: initial experience with brain tumors. Eur Radiol 2017; 27:306–314.
18. Le Bihan D, Breton E, Lallemand D, Aubin ML, Vignaud J, Laval-Jeantet M. Separation of diffusion and perfusion in intravoxel incoherent motion MR imaging. Radiology 1988; 168:497–505.
19. Jensen JH, Helpern JA, Ramani A, Lu H, Kaczynski K. Diffusional kurtosis imaging: the quantification of non-gaussian water diffusion by means of magnetic resonance imaging. Magn Reson Med 2005; 53:1432–1440.
20. Ding Y, Hazle JD, Mohamed AS, et al. Intravoxel incoherent motion imaging kinetics during chemoradiotherapy for human papillomavirus-associated squamous cell carcinoma of the oropharynx: preliminary results from a prospective pilot study. NMR Biomed 2015; 28: 1645–1654.
21. Fujima N, Yoshida D, Sakashita T, et al. Prediction of the treatment outcome using intravoxel incoherent motion and diffusional kurtosis imaging in nasal or sinonasal squamous cell carcinoma patients. Eur Radiol 2017; 27:956–965.
22. Hauser T, Essig M, Jensen A, et al. Characterization and therapy monitoring of head and neck carcinomas using diffusion-imaging-based intravoxel incoherent motion parameters-preliminary results. Neuroradiology 2013; 55:527–536.
23. Yun TJ, Kim JH, Kim KH, Sohn CH, Park SW. Head and neck squamous cell carcinoma: differentiation of histologic grade with standard- and high-b-value diffusion-weighted MRI. Head Neck 2013; 35:626–631.
24. Driessen JP, Caldas-Magalhaes J, Janssen LM, et al. Diffusion-weighted MR imaging in laryngeal and hypopharyngeal carcinoma: association between apparent diffusion coefficient and histologic findings. Radiology 2014; 272:456–463.